batteries

MDPI

Article

An Adaptable Capacity Estimation Method for Lithium-Ion Batteries Based on a Constructed Open Circuit Voltage Curve

Linjing Zhang, Xiaoqian Su, Caiping Zhang *, Yubin Wang, Yao Wang, Tao Zhu and Xinyuan Fan

National Active Distribution Network Technology Research Center (NANTEC), Beijing Jiaotong University, Beijing 100044, China; lj.zhang@bjtu.edu.cn (L.Z.); 24126295@bjtu.edu.cn (X.S.); 18117024@bjtu.edu.cn (Y.W.); 24126318@bjtu.edu.cn (Y.W.); taozhu@bjtu.edu.cn (T.Z.); 18117004@bjtu.edu.cn (X.F.)
* Correspondence: zhangcaiping@bjtu.edu.cn

Abstract

The inevitable decline in battery performance presents a major barrier to its widespread industrial application. Adaptive and accurate estimation of battery capacity is paramount for battery operation, maintenance, and residual value evaluation. In this paper, we propose a novel battery capacity estimation method based on an approximate open circuit voltage curve. The proposed method is rigorously tested using both lithium–iron–phosphate (LFP) and nickel–cobalt–manganese (NCM) battery packs at multiple charging rates under varied aging conditions. To further enhance capacity estimation accuracy, a voltage correction strategy is implemented utilizing the incremental capacity (IC) curve. This strategy also verifies the potential benefits of increasing the charging rate to shorten the overall test duration. Eventually, the capacity estimation error is consistently controlled within 2%. With optimal state of charge (SOC) interval selection, the estimation error can be further reduced to 1%. Clearly, our proposed method exhibits excellent compatibility across diverse battery materials and degradation states. This adaptability holds substantial scientific value and practical importance. It contributes to the safe and economic utilization of Li-ion batteries throughout their entire lifespan.

Keywords: lithium-ion battery; capacity estimation; open circuit voltage curve; lithium–iron–phosphate battery; nickel–cobalt–manganese battery; residual value evaluation

Academic Editor: Alessandro Lampasi

Received: 17 June 2025
Revised: 9 July 2025
Accepted: 12 July 2025
Published: 14 July 2025

Citation: Zhang, L.; Su, X.; Zhang, C.; Wang, Y.; Wang, Y.; Zhu, T.; Fan, X. An Adaptable Capacity Estimation Method for Lithium-Ion Batteries Based on a Constructed Open Circuit Voltage Curve. *Batteries* **2025**, *11*, 265. https://doi.org/10.3390/batteries11070265

1. Introduction

The rapid expansion and widespread adoption of electric vehicles (EVs) have fueled the dynamic development of Li-ion batteries [1]. However, inevitable battery performance degradation results in shorter EV driving ranges and heightens consumer anxiety. In extreme scenarios, severe faults may arise, posing security risks for EVs [2,3]. As batteries are used over time, it is necessary to evaluate the available capacity. Additionally, as numerous electric vehicles have been introduced to the market in recent years, the first generation of electric vehicles is now reaching retirement age [4]. If the capacities of these retired Li-ion batteries can be accurately evaluated and regrouped into battery packs with consistent performance, they can be repurposed as energy storage systems. Therefore, adaptive and accurate estimation for the battery capacities holds substantial scientific merit and practical significance to guarantee the safety and economic utilization of the Li-ion batteries during the whole lifespan.

The battery pack for EVs consists of numerous series-parallel connected unit cells. Although accurate capacity information is feasible by implementing a full charge and

discharge test for each cell, it is both time-consuming and cumbersome. To minimize test duration and costs, many scholars have delved into battery capacity or state-of-health (SOH) estimation methods. Broadly, these capacity estimation methods can be categorized into two groups: the Calculation Solution Method (CSM), which relies on models or model parameters, and the Training Learning Method (TLM), which leverages data. Correspondingly, the proposed models mainly include the empirical model, the open circuit voltage (OCV) curve model, the incremental capacity (IC) curve model, the equivalent circuit model (ECM), the electrochemical impedance spectroscopy (EIS) model, and the electrochemical model.

The accurate solution of the model itself frequently hinges on the empirical models [5,6] and electrochemical models. The empirical model necessitates extensive battery testing in controlled laboratory settings, taking into account various factors such as depth of discharge (DOD) [7], temperature, and current [8]. Once constructed, the empirical model is applied online through the interpolation method. However, the complex real-world operating conditions of Li-ion batteries introduce uncertainties in the degradation process, further compromising prediction accuracy. Subsequently, the parameters of the initial empirical model are refined with additional filters to minimize prediction errors [9].

The electrochemical model requires a deep understanding of the battery materials, structure, chemical reactions, and capacity degradation mechanisms [10]. It can simulate the internal properties and parameter changes of the battery. However, the electrochemical model has some intrinsic disadvantages with its complex structure, numerous parameters, and expensive calculation cost [11]. Hence, simplified methods of model structure and parameter-solving solutions are derived, including the reduced-order electrochemical model [12], the single-particle model [13], and the half-cell model [14]. Nevertheless, the dilemma of model accuracy and complexity persists, in which it is necessary to determine which model is more suitable for the design and development of battery manufacturing.

Parameter-based CSMs are explored to search for characteristic parameters strongly related to capacity with battery aging. They are an indirect method of estimating battery capacity, which relieves the constraints on the complexity of the models. Among the parameter-based CSMs, the simplest one is the battery voltage curve model [15,16]. Schmitt et al. quantified capacity fade using aged OCV [17]. The IC curve model is based on the differential capacity of the battery. Piao et al. [18] and Hong et al. [19] verified the effectiveness of capacity estimation using the characteristic parameters extracted from the IC curve. Although the information of the IC curve has a strong correlation with the battery capacity, the estimation results are affected by the current.

In addition to converting the battery voltage curve, the circuit model of the battery was also built [20–22]. The integer-order model [20] can only simulate the linear part of the model structure, with large prediction errors. Shi et al. [21] introduced the electrochemical theory to modify the model structure to improve accuracy. Consequently, the birth of the fractional-order circuit model [22] was used to accurately simulate the complex nonlinear part of the electrochemical reactions inside the batteries. Furthermore, the EIS model can be established by observing the voltage response in a wide frequency range, with a weak AC excitation current injection into the battery system [23]. This model expresses different processes of electrochemical reactions, and the battery capacity is estimated based on variation in the impedance characteristics [24–28]. Although the above-mentioned parameter-based method is easy to implement, subsequent capacity estimation errors will be amplified by the initial error results from the estimation of model parameters.

The data-based TLM employs sample data or past experience to program the machine without any models. A large amount of raw data is directly trained, after being transformed with mathematics/signal processing methods, to estimate capacity. In detail, various

machine learning methods, such as Deep Neural Networks (DNNs) [1] and support vector machines (SVMs) [29], are employed to directly estimate the battery capacity without considering the uncertainties. Moreover, Yang et al. have used a hierarchical data-driven framework that combines the feature matrix to achieve accurate SOH estimation [30]. Liu et al. [31] and Wang et al. [32] extract the highly representative features from OCV and IC for model training. The estimation results of the proposed methods are usually satisfactory. However, the data acquisition and feature extraction process will introduce additional noise, affecting the accuracy of the model [33].

All of the aforementioned capacity estimation methods can be applied online or offline. However, with the vigorous development of the Li-ion battery industry, the used material system and packaging structure are progressive. In addition, the performance degradation path and degradation mode of the batteries are complex and changeable depending on working conditions. Even more, the batteries may encounter sudden performance degradation. The fixed model structure and incomplete training data make it difficult to achieve accurate estimated capacity. Meanwhile, data-based methods require huge computing power and are difficult to apply online. Therefore, considering the uniformity of cell degradation in battery packs, this paper proposes a battery capacity estimation method based on approximate open circuit voltage curves, as well as incremental capacity curves for voltage correction. Relying on the definition of SOC, it can realize the adaptive and accurate estimation of battery capacity for different material systems and at different health states, which further enhances the safety, reliability, and use economy of Li-ion batteries.

The remaining content of this article will be described in the following five parts. Section 2 designs battery cell and module test experiments under different material systems and different aging states for the verification of the proposed capacity estimation method. The battery capacity estimation method based on the approximate OCV curve and the battery voltage correction principle based on the IC curve are described in Section 3. The capacity estimation accuracy and test efficiency of the proposed capacity estimation method are discussed in Section 4. Finally, the main contribution of this article is summarized.

2. Experiment Program of Li-Ion Batteries

The experiments are performed on the two most popular commercial batteries, ternary and lithium–iron–phosphate battery packs. The cathode materials are nickel–cobalt–manganese (NCM) and lithium–iron–phosphate (LFP), respectively, and both the anode materials are graphite. All experiments were carried out on the battery experiment platform composed of an Arbin battery test system (RePower 5 V-100 A, Arbin Instruments, Shenzhen, China), a PC, and a thermostat (Taisite biochemical incubator XP-250L, Taisite Lab Sciences Inc., Tianjin, China). Unless otherwise specified, the ambient temperature of the experiment was 25 °C. The LFP battery pack was a retired battery pack with a rated capacity of 160 Ah, and the grouping method was 8p4s. The charge and discharge voltage ranged from 2.5 V to 3.65 V, with a maximum continuous charging rate of 1C. When a battery pack is decommissioned, the capacity generally declines to 60% to 80% of its nominal capacity. To ensure the safety of the battery pack, a 0.2C charging current rate was applied and the unit cell voltage was limited to 3.65 V. If a unit cell was fully charged, the charging process would be stopped. And this cell would be regarded as the reference battery to ensure high-end alignment of the cell voltage. After that, the battery pack was discharged with a current of 0.5C until the voltage of any unit cell reached 2.5 V. If the cell reaching the discharge cut-off voltage was the same as the reference battery, the experiment was stopped. Otherwise, the reference battery continued to be discharged to 0% SOC to attain the SOC-OCV curve. In order to study the applicability of the battery capacity estimation method proposed in this paper under different material systems and aging conditions, the

new and aged NCM Li-ion battery cells were also selected and regrouped using the 1p4s strategy, respectively. The rated capacity of the cell was 8 Ah, the charge cut-off voltage was 4.2 V, and the discharge cut-off voltage was 2.8 V. The two ternary battery packs were subjected to the same test scheme as the LFP battery pack, except that the applied charging rate was 0.25C. Meanwhile, a number of experiments with different charging rates were designed and implemented to reduce the test cycle of the proposed method. The true capacity of each cell in the module was obtained by using cell test equipment to perform a complete 0.5C charge and discharge cycle to verify the accuracy of the proposed battery capacity estimation method. Triplicate measurements were performed for each test group to verify data consistency, and then the last cycle capacity was adopted. The detailed battery experiment number and program are shown in Table 1.

Table 1. Battery experiment scheme.

Material	Health Status	Battery Number	Charging Rate	Discharge Rate
Ternary (NCM)	New	PackA (Cells 1, 2, 3, 4)	0.25C 0.5C 1C	0.5C
	Aging	PackB (Cells 1, 2, 3, 4)	0.25C 0.5C 1C	0.5C
LFP	Aging	PackC (Cells 1, 2, 3, 4)	0.2C	0.5C

Statistics on the health status of the battery pack and the capacity distribution of the individual cells in the pack are shown in Figure 1. The average capacity of PackC obtained from retired LFP batteries is 143.328 Ah, with a corresponding rated capacity retention rate of 89.58%. When a retired battery pack is applied to energy storage systems, purchase costs can be effectively reduced to increase the utilization value, demonstrating the necessity of accurate capacity estimation. The average rated capacity retention rates of the regrouped PackA and PackB are 106.86% and 89.56%, respectively, and the health status of PackB is similar to PackC. However, it can be clearly observed from the health status distribution of the unit cells that PackC has better consistency than PackA and PackB. In detail, the variances of the rated capacity retention rates of PackC, PackA, and PackB are 0.198, 1.742, and 6.617, and the maximum deviations from the mean value are −0.62%, 1.71%, and −3.06%. The inconsistency ranking is PackB > PackA > PackC. The reassembled ternary lithium-ion battery packs have a worse inconsistency, which is convenient to verify the adaptive ability of the proposed capacity estimation method.

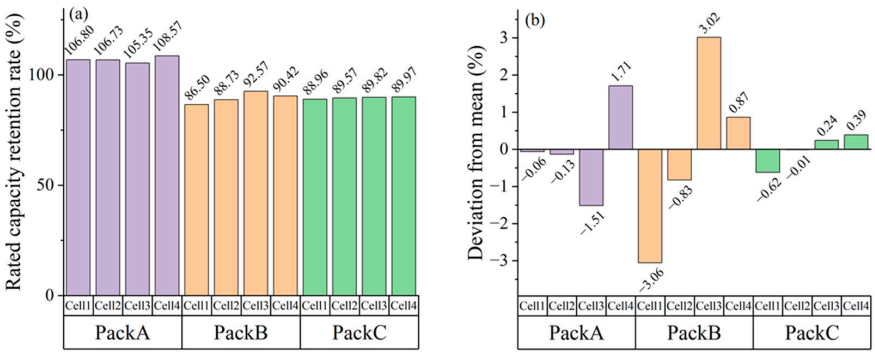

Figure 1. The health status distribution of the battery packs. (**a**) Rated capacity retention rate; (**b**) rated capacity retention rate deviating from the average value of the three battery packs.

3. Battery Capacity Estimation Method Based on the Approximate OCV

It is desirable to acquire the precise capacity of each unit cell in the battery pack in order to provide a supply for battery equalization and to improve the energy utilization ratio. Constrained by test time and cost, it is impractical for each cell in the battery pack to be fully charged and discharged. The method based on the approximate OCV curve can effectively estimate the capacity of each unit cell in the battery pack. How to attain the current approximate OCV curve of each cell is the key issue of this method. The OCV refers to the open circuit voltage of a battery. However, it is convenient to measure the terminal voltage of the batteries during the test but not for the OCV. The accurate open circuit voltage of the battery is usually obtained by letting it stand for a long time. However, the time-consuming test cycle is unacceptable. In addition to long-term standing, there is another way to calculate the approximate OCV curve by averaging the battery charge and discharge curves. The battery's electrical behavior is characterized by the Rint equivalent circuit model, which consists of an open-circuit voltage source in series with an internal resistance. Succinctly, when the excitation current passes through the lumped circuit model, the relationship between the battery terminal voltage and the excitation current (assuming that the charging current is positive and the discharging current is negative) satisfies the following equation:

$$U_{\mathrm{ch}} = \mathrm{OCV} + I_{\mathrm{ch}} \times R_{\mathrm{ch}} \tag{1}$$

$$U_{\mathrm{dis}} = \mathrm{OCV} + I_{\mathrm{dis}} \times R_{\mathrm{dis}} \tag{2}$$

In Equations (1) and (2), U_{ch} is the terminal voltage when the battery is charged, *I*ch is the charging current, and R_{ch} is the charging internal resistance. Similarly, U_{dis} is the terminal voltage when the battery is discharged, $\mathrm{I_{dis}}$ is the discharge current, and R_{dis} is the discharge internal resistance. Generally, through identifying the internal resistance of the battery at different SOC points, there is little difference between the charge and discharge internal resistance in practical application. However, the gap is very limited. Therefore, to simplify the estimation process and avoid complex parameter identification, this study proposes an approximate assumption. We assume that $\mathrm{R_{ch}}$ is approximately equal to $\mathrm{R_{dis}}$. Combined with the above Equations (1) and (2), the approximate open circuit voltage $\mathrm{OCV_{est}}$ can be derived:

$$\mathrm{OCV_{est}} = U_{\mathrm{ch}} - \frac{I_{\mathrm{ch}}}{I_{\mathrm{ch}} - I_{\mathrm{dis}}} \times (U_{\mathrm{ch}} - U_{\mathrm{dis}}) = U_{\mathrm{dis}} - \frac{I_{\mathrm{dis}}}{I_{\mathrm{ch}} - I_{\mathrm{dis}}} \times (U_{\mathrm{ch}} - U_{\mathrm{dis}}) \tag{3}$$

In the process of the regular inspection and maintenance of electric vehicles or the residual value assessment of second-hand and decommissioned vehicles, the battery pack is first charged to 100% SOC. Secondly, discharging the battery pack to the voltage of any unit cell reaching the discharge cut-off voltage, and then continuing to discharge the fully charged cell through the equalization device until 0% SOC. Due to the inconsistency of the capacity distribution of the unit cells in the group, some of the battery cells may not have been fully charged since the charging process finished once one of the cells reached the upper cut-off voltage. In addition, the SOC at the beginning of battery charging is unknown, so only part of the Q-$\mathrm{OCV_{est}}$ curve of each unit cell can be extracted. And the actual discharge capacity $\mathrm{Q_0}$ of a fully charged battery cell and the partial discharge capacity Qpi of other cells in the group can be recorded. Finally, based on $\mathrm{Q_0}$, the Q-$\mathrm{OCV_{est}}$ curve of the fully charged cell can be converted into an SOC-$\mathrm{OCV_{est}}$ curve, with a 100% SOC point but a lack of low SOC.

Given the similar working conditions experienced by each cell in the battery pack before retirement, the capacity distribution is consistent and is achieved through PackC in Figure 1. It can be assumed that the SOC-$\mathrm{OCV_{est}}$ curve of each unit cell in the battery

pack is uniform. Furthermore, the SOC-OCV_{est} curve of one unit cell can be regarded as a representative SOC-OCV_{est} curve for all the other cells. By determining the charged or discharge capacity and varied SOC range of the not fully charged unit cells, the actual capacity can be calculated. The algorithm diagram is shown in Figure 2. In the previous description, the partial SOC-OCV_{est} curve of a fully charged battery has been extracted based on total discharge capacity; herein, this partial SOC-OCV_{est} curve is used as a reference. Taking PackC as an example, Cell 4 is selected as the reference battery since it is fully charged, and the capacity of Cell 2, which is not fully charged, is estimated. After that, specify the start and end OCV of the Q-OCV_{est} curve segment of Cell 2 in Figure 2b, denoted as OCV_{start} and OCV_{end}, then search for their corresponding capacities, Q_{start} and Q_{end}. Ultimately, determine the SOC_{start} and SOC_{end} corresponding to OCV_{start} and OCV_{end} on the benchmark SOC-OCV_{est} curve in Figure 2a, and the actual discharge capacity Q_r of Cell 2 can be estimated as follows:

$$Q_r = (Q_{end} - Q_{start}) / (SOC_{end} - SOC_{start}) \quad (4)$$

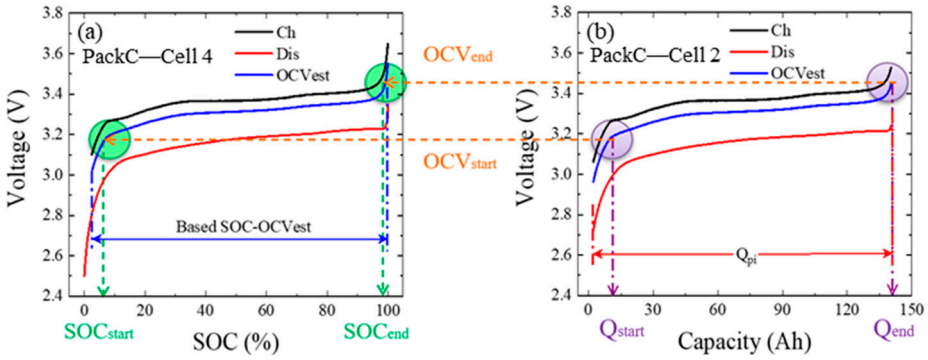

Figure 2. Schematic diagrams of the algorithm based on the OCV_{est} curve. (**a**) The extracted SOC-OCV_{est} curve of the reference battery, which is fully charged. (**b**) The calculated Q-OCV_{est} curve of the battery whose capacity is to be estimated.

For the proposed battery capacity estimation method, a critical aspect is to determine the OCV_{est} correlation between the reference battery and the capacity-estimated battery. Ideally, the OCV_{est} in the reference SOC-OCV_{est} curve is identical to that in the Q-OCV_{est} curve of the battery to be estimated, as shown in Figure 2. In fact, there are measurement errors from the battery pack test equipment: a data recording error and a slight inconsistency between unit cells. Therefore, the corresponding OCV_{est} needs to be corrected. The Q-OCV_{est} curve of the battery is relatively flat, and it is difficult to determine the voltage characteristics. Based on the incremental capacity (IC) curve, which captures the differential voltage response during charging and discharging, the electrochemical reaction process can be distinctly reflected. Simultaneously, obvious peak and valley features in the IC curve are easy to identify. For LFP Li-ion batteries, the characteristic peaks of the IC curve are mainly supported by the graphite negative electrode. According to different phase transition reactions, the IC curve can be divided into five characteristic peaks, including the obvious peak ①, peak ②, and peak ⑤, as well as weak peak ③ and peak ④. Therein, peak ① and peak ② are the most significant, and the peak intensity is much greater than in other peaks. By comparison with the battery's Q-OCV_{est} curve, all the corresponding voltage ranges to each IC peak are around 40 mV, as presented in Figure 3. The peak intensity variation of the IC curve significantly amplifies the negligible voltage change in the Q-OCV_{est} curve and incarnates the voltage change characteristics resulting from the electrochemical reaction mechanism. Therefore, the IC curve peak can be employed to perform OCV_{est} correction, further effectively eliminating the error impacts.

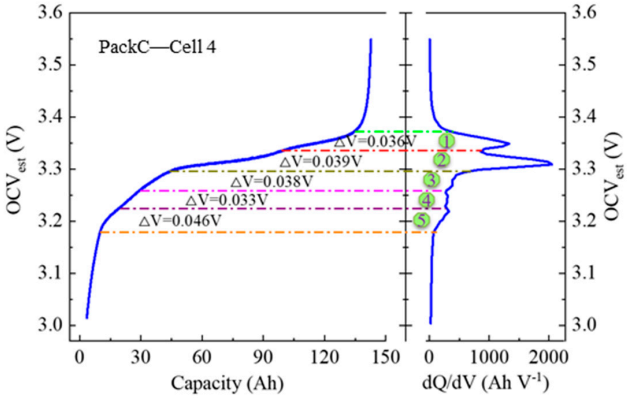

Figure 3. The corresponding relationship between the Q-OCV_{est} curve and the IC curve of the LFP battery.

The corrected algorithm diagram is illustrated in Figure 4, and the flowchart of the self-adaptive and accurate capacity estimation method for the lithium-ion battery pack is displayed in Figure 5. The method of voltage correction for PackC includes the process of curve differentiation–normalization–translation. In detail, the first step is to perform differential calculation on the Q-OCV_{est} curve of the reference battery and the battery to be estimated to attain the corresponding IC curve, which is recorded as IC_0 and IC_i, as shown in Figure 4a. The second step is to normalize IC_0 and IC_i according to their strongest peak intensities, y_0 and y_i. The last step is to translate IC_i by the voltage gap ΔV of the two strongest peaks so that the position of the peak ② of IC_i coincides with that of IC_0. Afterwards, the OCV_{end} and OCV_{start} for the cell to be estimated, specified in Figure 2, can be corrected according to the translation amount ΔV to obtain the modified OCV_{end}' and OCV_{start}'. Finally, the SOC_{end}' and SOC_{start}' corresponding to the OCV_{end}' and OCV_{start}' in the reference SOC-OCV_{est} curve must be searched for in order to estimate the corrected actual discharge capacity Q_r':

$$Q_r' = (Q_{end} - Q_{start}) / (SOC_{end}' - SOC_{start}') \quad (5)$$

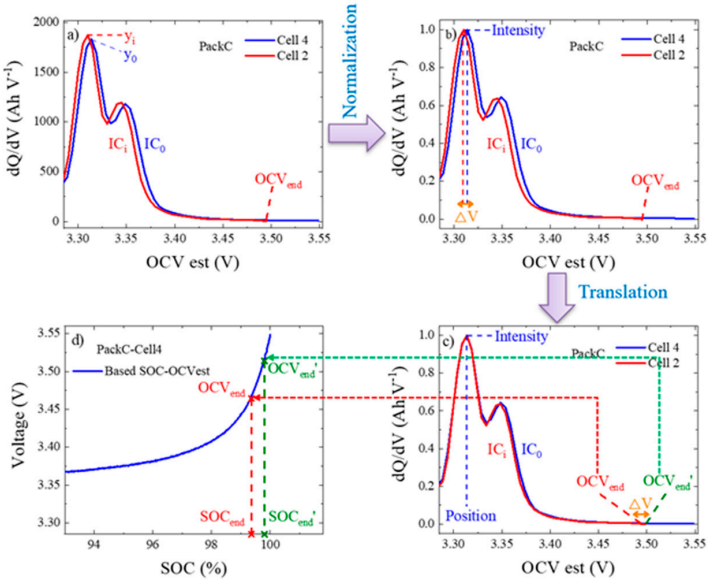

Figure 4. An algorithm diagram of the battery voltage correction principle based on the IC curve. (**a**) Differential of the Q-OCV_{est} curve of the battery to be estimated and the reference battery; (**b**) normalization and (**c**) translation of the IC curve; and (**d**) verification of the corrected corresponding SOC in the reference SOC-OCV_{est} curve.

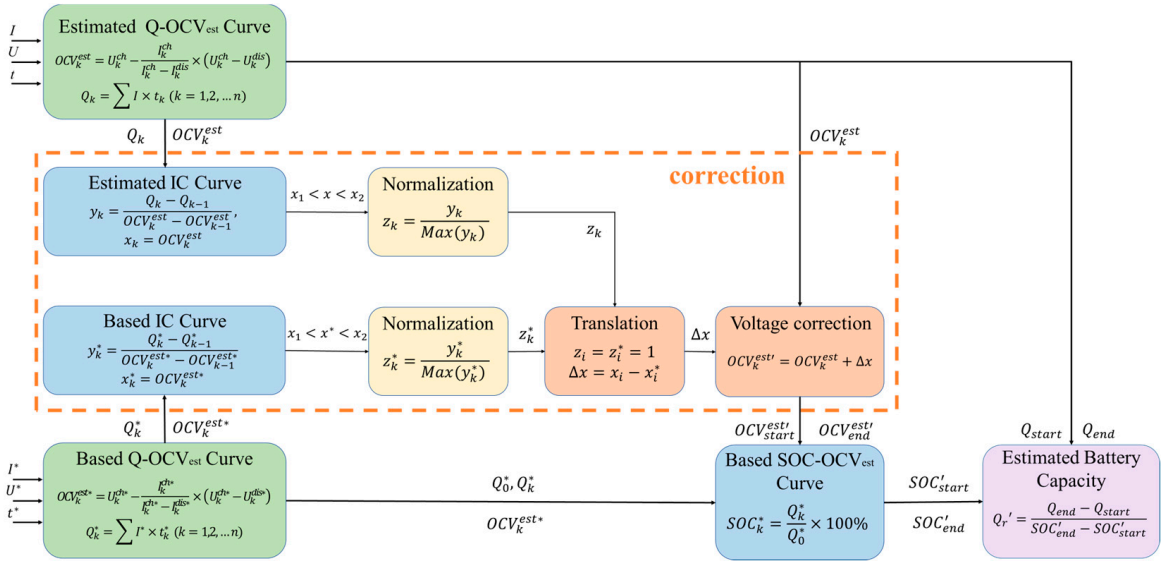

Figure 5. A flowchart of the self-adaptive and accurate capacity estimation method for a small-scale Li-ion battery pack.

4. Results and Discussion

4.1. Capacity Estimation Results of LFP Battery

The proposed capacity estimation method is implemented to estimate the capacity of PackC cells. Cell 4 is determined as the reference battery, and the remaining cells are the estimated batteries. Since the initial SOC of each cell is uncertain at the beginning of charging in applications, it is necessary to discuss the capacity estimation accuracy using different SOC intervals. As described in Section 3, the SOC intervals of different electrochemical processes can be divided into several segments based on the IC curves. From Figure 3, the charging process exhibits five characteristic IC peaks. It can be seen that the intensity of peak ③ and peak ④ are too weak, making them hard to identify. Therefore, their characteristics are ignored when selecting the SOC intervals, and only three characteristic peaks, peak ①, peak ②, and peak ⑤, are employed. Figure 6 illustrates that the whole charging curve is divided into seven SOC intervals according to the characteristics of the IC curve. The specific division results are illustrated in Table 2. In the subsequent capacity estimation, the capacity of one or more sequent SOC intervals is employed to estimate the overall capacity of the battery.

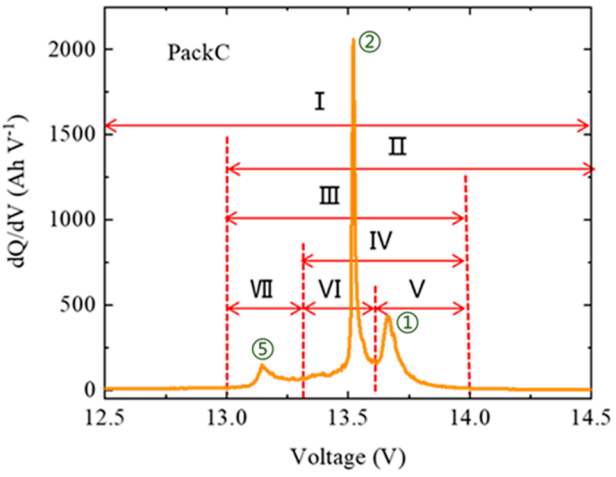

Figure 6. Division of interval for estimation of LFP battery capacity based on battery pack IC curve.

Table 2. Detailed rules for dividing the SOC interval of cell capacity estimation.

Number	Symbol	Voltage Range	ΔSOC
1	I	Start voltage–Cut-off voltage	≈100%
2	II	13.0 V–Cut-off voltage	≈92%
3	III	13.0 V–14.0 V	≈90%
4	IV	13.3 V–14.0 V	≈75%
5	V	13.6 V–14.0 V	≈30%
6	VI	13.3 V–13.6 V	≈45%
7	VII	13.0 V–13.3 V	≈15%

The capacity of each cell in the battery module is estimated based on the above-mentioned seven SOC intervals, and different battery capacity estimation results can be derived. Figure 7 reveals the capacity estimation results and error analysis of each cell in PackC using different SOC intervals before and after the OCV_{est} correction. It can be seen that the capacity estimation error before the OCV_{est} correction is partially over the limit, especially with the three independent IC peaks, namely, interval V, interval VI, and interval VII. Compared with these three intervals, the capacity estimation error of interval VI and interval VII is relatively shallow, while the error of interval V is up to 8%. After the OCV_{est} correction, the estimated capacity is more accurate, and the capacity estimation error is reduced to less than 2%, even using each independent IC peak. It can be demonstrated that for LFP batteries, the OCV_{est} correction based on the IC curve can effectively ameliorate the accuracy of capacity estimation. However, regardless of whether the battery OCV_{est} is corrected or not, capacity estimation accuracy is improved with an increased SOC interval range. When the selected SOC segments involve the three voltage platforms together, the estimation error is basically within 0.5%. With only an independent voltage platform, the estimation error can increase to 1% or higher. It can be concluded that when all three characteristic peaks on the IC curve, peak ①, peak ② and peak ⑤, are selected for the LFP battery, a high capacity estimation accuracy can be obtained. However, it is a waste of time and the charging segment usually cannot cover such a wide voltage range in practical applications. Therefore, in order to balance the consumption time and the estimation accuracy, it is feasible to choose the voltage range corresponding to only the two characteristic peaks of peak ① and peak ② on the IC curve or the independent characteristic peak through the proposed correction method.

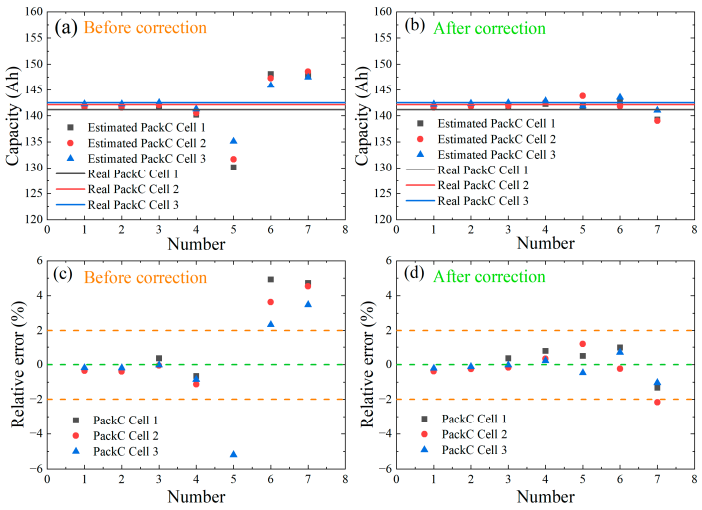

Figure 7. Capacity estimation results and error distribution with the proposed method for an LFP battery: the estimated result of battery capacity (**a**) before correction and (**b**) after correction; the relative error of the estimated battery capacity (**c**) before correction and (**d**) after correction.

4.2. Capacity Estimation Results of NCM Li-Ion Battery

At present, the NCM ternary Li-ion battery has also been widely used for EVs and energy storage because of its higher voltage platform, greater specific energy, and longer cycle life. PackA, listed in Table 1, is the new NCM ternary Li-ion battery for capacity estimation. As described in Section 2, the initially fully charged cell is served as the reference. In this pack, Cell 3 is fully charged first; therefore, it is regarded as the reference battery. The relationship between the corresponding Q-OCV_{est} curve and IC curve is represented in Figure 8. The total IC curve is mainly composed of three parts, including the phase-transformation characteristic peak ② and peak ③ and the relatively broad and flat solid-solution region ①. In which the electrochemical reactions in peak ② and the solid-solution region ① contribute about 70% of the entire charging capacity. Compared with the LFP battery, the number of characteristic peaks of the IC curve is reduced, and the voltage variation range corresponding to each segment is correspondingly broadened. Based on the characteristics of the OCV_{est} curve, the above-proposed capacity estimation method is carried out for PackA. Considering the influence of different SOC usage intervals, the OCV_{est} of each cell at the end of the battery pack charging is selected as OCV_{end}, and the battery capacity estimation effect is observed by changing the OCV_{start} (Figure 8). The OCV_{start} of 2.8 V means that the battery pack is completely empty, and an OCV_{est} is selected as the OCV_{start} at 0.1 V intervals from 3.4 V to 4 V. The capacity estimation result and its error distribution without OCV_{est} correction are exhibited in Figure 9. For a different OCV_{start}, the capacity estimation error of each cell is all within 2%, which has a sufficiently high estimation accuracy. When the selected OCV_{start} does not exceed 3.6 V, and the interval includes both the characteristic peak ② and the solid-solution area ①, the capacity estimation error can even be reduced to less than 1%. Once OCV_{start} reaches 3.7 V, the information on peak ②, which dominates the phase-change reaction, is no longer detectable. As a result, the difference in the partial SOC-OCV_{est} curve among the individual cells in the battery pack is enlarged, and the capacity estimation result becomes relatively poor. The above-proposed correction method for the LFP battery is based on the characteristic peak of the IC curve. For NCM ternary batteries, when the OCV_{start} reaches 3.7 V, the characteristic IC peak disappears, only represented as a flat solid solution region. Thus, it brings inapplicability due to difficulty in finding the key characteristic values. Fortunately, the estimation accuracy of the proposed method without correction is sufficient to meet practical requirements. Correspondingly, in the view of the SOC scale, when the initial charging SOC is lower than 50%, a higher estimation accuracy can be achieved. In practical applications, if there is a strict requirement for estimation accuracy for ternary batteries, the selected starting SOC should be below 50%. Supposing that the program period is limited, the charging voltage or starting SOC can be further promoted without sacrificing much accuracy.

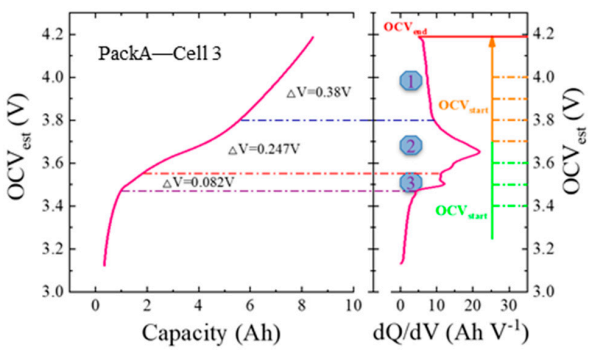

Figure 8. The corresponding relationship between the Q-OCV_{est} curve and the IC curve of the new NCM battery.

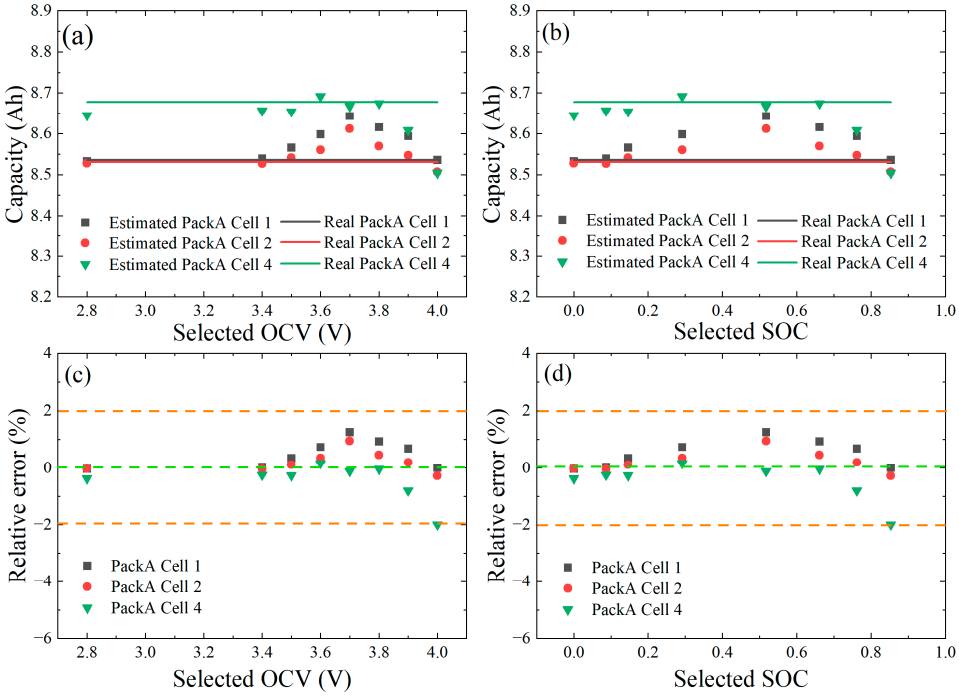

Figure 9. Capacity estimation results and error distribution for the new NCM battery: the capacity estimation results without OCV_{est} correction on (**a**) the OCV scale and (**b**) the SOC scale; the corresponding relative error on the (**c**) OCV scale and (**d**) the SOC scale.

The application of the proposed capacity estimation method in both the new NCM ternary and aged LFP battery systems has been analyzed. However, it is also necessary to know the cell capacity when the NCM batteries are put into service for some time. Therefore, the NCM battery after aging is also regrouped, and the adaptability of the method on the aged batteries is further explored. Similarly, Cell 1 in PackB is fully charged first and then regarded as the reference battery, and the capacity of other cells is to be estimated. The estimation results and error distribution are shown in Figure 10. It can be clearly observed that the capacity estimation error of the aged NCM battery sharply increases while the initial SOC increases to approximately 50%. The maximal absolute error is up to 6.65%. The capacity estimation results of Packs A, B, and C are shown in Tables 3–5. Compared with PackC, even under the same rated capacity retention rate, the capacity estimation error appears larger due to the expansion of the inconsistency of PackB. However, even if the battery consistency differs by 30 times, when the initial SOC does not exceed 40%, the estimated error can still be kept within 2%. Given that the initial SOC during battery operation typically remains below 40%, the proposed method is still effective on aged batteries.

From the capacity estimation results on the three types of battery packs, it can be proved that accurate capacity estimation can be ensured when selecting an appropriate initial SOC for charging. During the above tests, a low current is applied when charging the battery pack. However, it is also hoped to curtail the test time and cut down the test cost on the premise of certain capacity estimation accuracy. After speeding up the charging rate from 0.25C to 0.5C and 1C, the proposed method is continued to be employed to estimate the capacity of NCM battery packs in two health states. Take the largest absolute capacity estimation error of the battery to be estimated; the influence of the charging rate on the battery capacity estimation result is discussed, as indicated in Figure 11. As the charging rate increases, the capacity estimation error of each cell in PackA does not change significantly, and it can still maintain a good effect within 1%. In contrast to PackA, the capacity estimation result of PackB after aging is relatively more affected by

the charging rate. Although the charging rate is increased by four times, the maximum capacity estimation error is only 2.5%, which is satisfactory. Under the premise of fulfilling the estimation accuracy, it is gratifying for the proposed capacity estimation method to effectively promote the test efficiency by improving the charging rate.

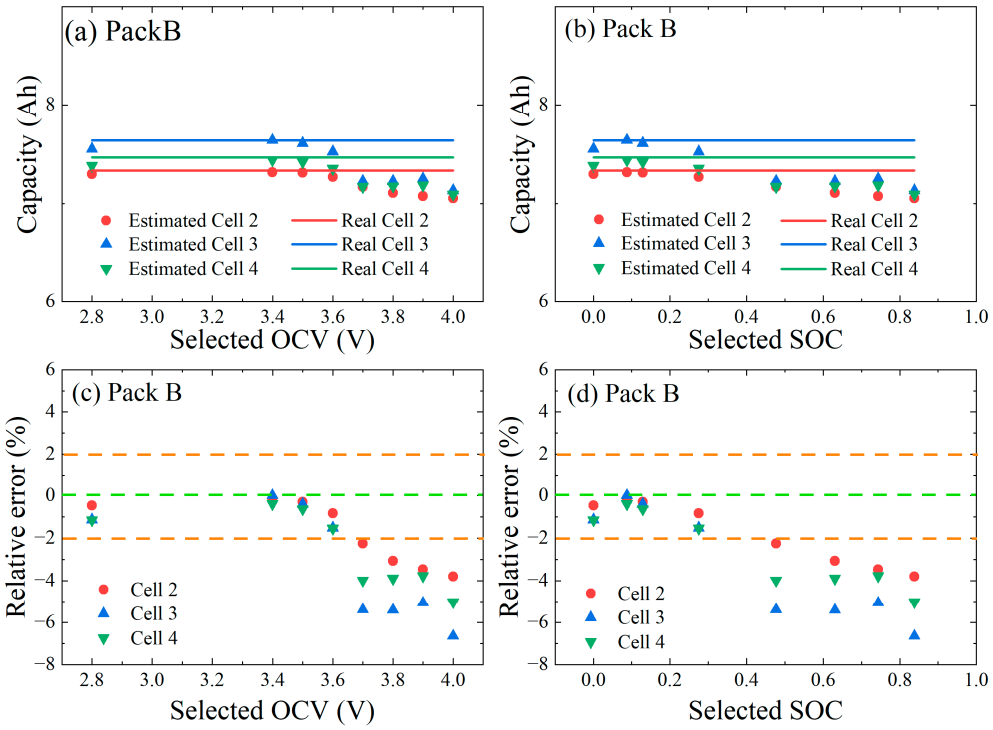

Figure 10. Capacity estimation results and error distribution for an aged NCM battery with the proposed method: the capacity estimation results without OCV_{est} correction on (**a**) the OCV scale and (**b**) the SOC scale; the relative error of the estimated battery capacity on (**c**) the OCV scale and (**d**) the SOC scale.

Table 3. The capacity estimation results of PackC.

Material	**Health Status**	**Battery Number**	**Reference Battery**
LFP	Aging	PackC (Cell 1, 2, 3, 4)	Cell 4
ΔSOC	**Estimation Error**		
	PackC Cell 1	**PackC Cell 2**	**PackC Cell 3**
≈100%	/	−0.39%	−0.22%
≈92%	/	−0.25%	−0.12%
≈90%	0.36%	−0.17%	−0.03%
≈75%	−0.78%	0.33%	−0.22%
≈30%	0.50%	1.17%	−0.47%
≈45%	0.98%	−0.24%	0.70%
≈15%	−1.32%	−2.16%	−1.04%

In general, except for the seriously aged NCM battery at a high initial charging SOC, the proposed method has strong adaptive ability for batteries with different material systems. The estimation error can be kept within 2%. By selecting the appropriate SOC interval, the estimation accuracy can be further promoted to within 1%, which is more accurate than the current feature extraction method [4]. For the LFP battery pack, the strategy of OCV_{est} correction based on the IC curve is adopted to improve the proposed method. In order to enhance the test efficiency, when the selected SOC range includes the

characteristic peak ① and peak ② or the independent characteristic peak on the IC curve, the estimation error within 2% can be achieved. For the NCM battery pack, the test time can be shortened by increasing the charging rate, with the capacity estimation error of PackA within 1%. Unfortunately, the aged ternary PackB's estimation accuracy is affected by the charging rate, and the error is within 2.5%. The proposed method can simply realize fast, high-precision single-cell capacity estimation in a battery pack. However, the method of correcting the error caused by the expansion of the consistency difference still needs further research.

Table 4. The capacity estimation results of PackA.

Material	Health Status	Battery Number	Reference Battery
NCM	New	PackA (Cells 1, 2, 3, 4)	Cell 3
Initial SOC	**Estimation Error**		
	PackA Cell 1	**PackA Cell 2**	**PackA Cell 4**
0	−0.03%	−0.03%	−0.38%
≈8.7%	0.04%	−0.05%	−0.25%
≈14.6%	0.35%	0.12%	−0.27%
≈29.2%	0.74%	0.35%	0.16%
≈51.8%	1.26%	0.96%	−0.12%
≈66.1%	0.93%	0.46%	−0.04%
≈76.2%	0.68%	0.20%	−0.80%
≈85.3%	0.0007%	−0.28%	−2.00%

Table 5. The capacity estimation results of PackB.

Material	Health Status	Battery Number	Reference Battery
NCM	Aging	PackB (Cells 1, 2, 3, 4)	Cell 1
Initial SOC	**Estimation Error**		
	PackB Cell 2	**PackB Cell 3**	**PackB Cell 4**
0	−0.47%	−1.13%	−1.15%
≈8.7%	−0.25%	0.009%	−0.39%
≈12.9%	−0.29%	−0.40%	−0.64%
≈27.5%	−0.84%	−1.52%	−1.55%
≈47.7%	−2.24%	−5.39%	−3.99%
≈63.1%	−3.08%	−5.41%	−3.90%
≈74.3%	−3.48%	−5.06%	−3.78%
≈83.8%	−3.81%	−6.65%	−5.02%

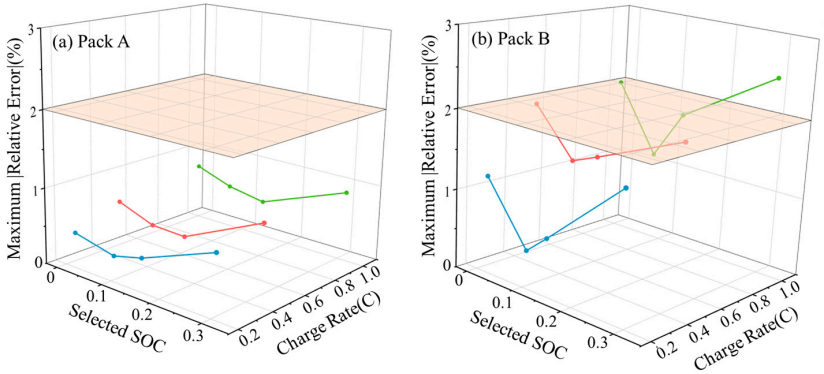

Figure 11. The influence of the charging rate on the battery capacity estimation result.

5. Conclusions

Performance decline is inevitable with the life-time service of Li-ion batteries. Meanwhile, capacity variance would appear in the battery pack due to inconsistency between individual batteries. Therefore, it is essential to acquire the single-cell capacity in a battery pack to supply strategies for improving the energy utilization. Herein, an adaptive capacity estimation method is proposed based on LFP and NCM batteries. Then the capacity estimation accuracy and test efficiency are assessed. The main contributions are as follows:

(1) An accurate capacity estimation method for Li-ion batteries without parameter identification is proposed. Under limited aging conditions, the proposed method remains effective across different battery material systems when an appropriate initial SOC and a high-repeatability reference battery are selected.

(2) The LFP battery's capacity is estimated based on the OCV_{est} curve, and the strategy of OCV_{est} correction based on the IC curve is implemented to improve the capacity estimation accuracy and test efficiency. The estimation error for aged batteries does not exceed 2%.

(3) The reaction characteristics of the NCM Li-ion battery are analyzed. By choosing a suitable initial SOC, the battery capacity estimation error is guaranteed to be within 2%. Furthermore, while considering safety and aging constraints, increasing the charging rate to shorten the program period has proved feasible.

The development of battery management systems has enabled systematic integration of active balancing devices, allowing independent operation of individual cells. The proposed capacity estimation method offers straightforward implementation and computational efficiency. Furthermore, the estimation results can directly inform adaptive balancing strategies. Subsequent work will focus on feedback mechanisms to correct for cell variations and temperature effects.

Author Contributions: Conceptualization, L.Z. and C.Z.; methodology, Y.W. (Yubin Wang); software, X.S.; validation, Y.W. (Yubin Wang), X.F. and X.S.; formal analysis, T.Z.; investigation, X.F.; resources, Y.W. (Yubin Wang); data curation, T.Z.; writing—original draft preparation, Y.W. (Yao Wang); writing—review and editing, X.S.; visualization, Y.W. (Yao Wang); supervision, L.Z.; project administration, L.Z.; funding acquisition, L.Z. All authors have read and agreed to the published version of the manuscript.

Funding: This research is supported by the National Natural Science Foundation of China (Grant No. 52222708).

Data Availability Statement: The data presented in this study are available on request from the corresponding author. The data are not publicly available due to the confidentiality of ongoing projects.

Conflicts of Interest: The authors declare no conflicts of interest.

References

1. Lu, J.; Xiong, R.; Tian, J.; Wang, C.; Sun, F. Deep Learning to Estimate Lithium-Ion Battery State of Health without Additional Degradation Experiments. *Nat. Commun.* **2023**, *14*, 2760. [CrossRef] [PubMed]
2. Shen, Y.; Wang, X.; Jiang, Z.; Luo, B.; Chen, D.; Wei, X.; Dai, H. Online Detection of Lithium Plating Onset during Constant and Multistage Constant Current Fast Charging for Lithium-Ion Batteries. *Appl. Energy* **2024**, *370*, 123631. [CrossRef]
3. Bhaskar, K.; Kumar, A.; Bunce, J.; Pressman, J.; Burkell, N.; Rahn, C.D. Data-Driven Thermal Anomaly Detection in Large Battery Packs. *Batteries* **2023**, *9*, 70. [CrossRef]
4. Fan, W.; Jiang, B.; Wang, X.; Yuan, Y.; Zhu, J.; Wei, X.; Dai, H. Enhancing Capacity Estimation of Retired Electric Vehicle Lithium-Ion Batteries through Transfer Learning from Electrochemical Impedance Spectroscopy. *eTransportation* **2024**, *22*, 100362. [CrossRef]
5. Jiang, Y.; Zhang, J.; Xia, L.; Liu, Y. State of Health Estimation for Lithium-Ion Battery Using Empirical Degradation and Error Compensation Models. *IEEE Access* **2020**, *8*, 123858–123868. [CrossRef]

6. Singh, P.; Chen, C.; Tan, C.M.; Huang, S.-C. Semi-Empirical Capacity Fading Model for SoH Estimation of Li-Ion Batteries. *Appl. Sci.* **2019**, *9*, 3012. [CrossRef]
7. Kong, L.; Fang, S.; Niu, T.; Chen, G.; Liao, R. A Capacity Degradation Estimation Error Correction Method for Lithium-Ion Battery Considering the Effect of Sequential Depth of Discharge. In Proceedings of the 2023 IEEE/IAS Industrial and Commercial Power System Asia (I & CPS Asia), Chongqing, China, 7–9 July 2023; IEEE: New York, NY, USA, 2023; pp. 1–7.
8. Jia, X.; Zhang, C.; Wang, L.Y.; Zhang, L.; Zhang, W. The Degradation Characteristics and Mechanism of $Li[Ni_{0.5}Co_{0.2}Mn_{0.3}]O_2$ Batteries at Different Temperatures and Discharge Current Rates. *J. Electrochem. Soc.* **2020**, *167*, 02050. [CrossRef]
9. Xue, Z.; Zhang, Y.; Cheng, C.; Ma, G. Remaining Useful Life Prediction of Lithium-Ion Batteries with Adaptive Unscented Kalman Filter and Optimized Support Vector Regression. *Neurocomputing* **2020**, *376*, 95–102. [CrossRef]
10. Chen, S.; Zhang, Q.; Wang, F.; Wang, D.; He, Z. An Electrochemical-Thermal-Aging Effects Coupled Model for Lithium-Ion Batteries Performance Simulation and State of Health Estimation. *Appl. Therm. Eng.* **2024**, *239*, 122128. [CrossRef]
11. Jana, A.; Mitra, A.S.; Das, S.; Chueh, W.C.; Bazant, M.Z.; García, R.E. Physics-Based, Reduced Order Degradation Model of Lithium-Ion Batteries. *J. Power Sources* **2022**, *545*, 231900. [CrossRef]
12. Gao, T.; Lu, W. Reduced-Order Electrochemical Models with Shape Functions for Fast, Accurate Prediction of Lithium-Ion Batteries under High C-Rates. *Appl. Energy* **2024**, *353*, 12195. [CrossRef]
13. Gu, Y.; Wang, J.; Chen, Y.; Xiao, W.; Deng, Z.; Chen, Q. A Simplified Electro-Chemical Lithium-Ion Battery Model Applicable for in Situ Monitoring and Online Control. *Energy* **2023**, *264*, 126192. [CrossRef]
14. Couto, L.D.; Charkhgard, M.; Karaman, B.; Job, N.; Kinnaert, M. Lithium-Ion Battery Design Optimization Based on a Dimensionless Reduced-Order Electrochemical Model. *Energy* **2023**, *263*, 125966. [CrossRef]
15. Yang, D.; Zhang, X.; Pan, R.; Wang, Y.; Chen, Z. A Novel Gaussian Process Regression Model for State-of-Health Estimation of Lithium-Ion Battery Using Charging Curve. *J. Power Sources* **2018**, *384*, 387–395. [CrossRef]
16. Qian, K.; Huang, B.; Ran, A.; He, Y.-B.; Li, B.; Kang, F. State-of-Health (SOH) Evaluation on Lithium-Ion Battery by Simulating the Voltage Relaxation Curves. *Electrochim. Acta* **2019**, *303*, 183–191. [CrossRef]
17. Schmitt, J.; Rehm, M.; Karger, A.; Jossen, A. Capacity and Degradation Mode Estimation for Lithium-Ion Batteries Based on Partial Charging Curves at Different Current Rates. *J. Energy Storage* **2023**, *59*, 106517. [CrossRef]
18. Piao, C.; Sun, R.; Chen, J.; Liu, M.; Wang, Z. A Feature Extraction Approach for State-of-Health Estimation of Lithium-Ion Battery. *J. Energy Storage* **2023**, *73*, 108871. [CrossRef]
19. Hong, J.; Chen, Y.; Chai, Q.; Lin, Q.; Wang, W. State-of-Health Estimation of Lithium-Ion Batteries Using a Novel Dual-Stage Attention Mechanism Based Recurrent Neural Network. *J. Energy Storage* **2023**, *72*, 109297. [CrossRef]
20. Fang, L.; Li, J.; Peng, B. Online Estimation and Error Analysis of Both SOC and SOH of Lithium-Ion Battery Based on DEKF Method. *Energy Procedia* **2019**, *158*, 3008–3013. [CrossRef]
21. Shi, M.; Yuan, J.; Dong, L.; Zhang, D.; Li, A.; Zhang, J. Combining Physicochemical Model with the Equivalent Circuit Model for Performance Prediction and Optimization of Lead-Acid Batteries. *Electrochim. Acta* **2020**, *353*, 136567. [CrossRef]
22. Guo, W.; Wang, Q.; Li, G.; Xie, S. Dual-Time Scale Collaborative Estimation of SOC and SOH for Lithium-Ion Batteries Based on FOMIRUKF-EKF. *Comput. Electr. Eng.* **2025**, *123*, 110048. [CrossRef]
23. Ando, K.; Matsuda, T.; Imamura, D. Degradation Diagnosis of Lithium-Ion Batteries with a $LiNi_{0.5}Co_{0.2}Mn_{0.3}O_2$ and $LiMn_2O_4$ Blended Cathode Using DV/DQ Curve Analysis. *J. Power Sources* **2018**, *390*, 278–285. [CrossRef]
24. Abu Qahouq, J. An Electrochemical Impedance Spectrum-Based State of Health Differential Indicator with Reduced Sensitivity to Measurement Errors for Lithium–Ion Batteries. *Batteries* **2024**, *10*, 368. [CrossRef]
25. Gao, Z.; Jin, Y.; Zhang, Y.; Zhang, Z.; Li, S.; Liu, J.; Wang, H. Static EIS Multi-Frequency Feature Points Combined with WOA-BP Neural Network for Li-Ion Battery SOH Estimation. *Measurement* **2025**, *253*, 117780. [CrossRef]
26. Wang, S.; Tang, J.; Xiong, B.; Fan, J.; Li, Y.; Chen, Q.; Xie, C.; Wei, Z. Comparison of Techniques Based on Frequency Response Analysis for State of Health Estimation in Lithium-Ion Batteries. *Energy* **2024**, *304*, 132077. [CrossRef]
27. Wu, J.; Meng, J.; Lin, M.; Wang, W.; Wu, J.; Stroe, D.-I. Lithium-Ion Battery State of Health Estimation Using a Hybrid Model with Electrochemical Impedance Spectroscopy. *Reliab. Eng. Syst. Saf.* **2024**, *252*, 110450. [CrossRef]
28. Li, C.; Yang, L.; Li, Q.; Zhang, Q.; Zhou, Z.; Meng, Y.; Zhao, X.; Wang, L.; Zhang, S.; Li, Y.; et al. SOH Estimation Method for Lithium-Ion Batteries Based on an Improved Equivalent Circuit Model via Electrochemical Impedance Spectroscopy. *J. Energy Storage* **2024**, *86*, 111167. [CrossRef]
29. Patil, S.; Havaldar, S.M.; Mathad, S.; Patil, K.R. Lithium-Ion Battery State of Health Estimation Using Support Vector Regression (SVR). In Proceedings of the 2023 International Conference on Ambient Intelligence, Knowledge Informatics and Industrial Electronics (AIKIIE), Ballari, India, 2–3 November 2023; IEEE: New York, NY, USA; pp. 1–6.
30. Yang, S.; Zhang, C.; Chen, H.; Wang, J.; Chen, D.; Zhang, L.; Zhang, W. A Hierarchical Enhanced Data-Driven Battery Pack Capacity Estimation Framework for Real-World Operating Conditions with Fewer Labeled Data. *J. Energy Chem.* **2024**, *91*, 417–432. [CrossRef]

31. Liu, H.; Deng, Z.; Che, Y.; Xu, L.; Wang, B.; Wang, Z.; Xie, Y.; Hu, X. Big Field Data-Driven Battery Pack Health Estimation for Electric Vehicles: A Deep-Fusion Transfer Learning Approach. *Mech. Syst. Signal Process* **2024**, *218*, 111585. [CrossRef]
32. Wang, J.; Zhang, C.; Meng, X.; Zhang, L.; Li, X.; Zhang, W. A Novel Feature Engineering-Based SOH Estimation Method for Lithium-Ion Battery with Downgraded Laboratory Data. *Batteries* **2024**, *10*, 139. [CrossRef]
33. Chen, G.; Wang, C.; Yang, Y.; Zhang, X.; Deng, W.; Liu, J. Online Condition Monitoring and State of Health Estimation Method for Lithium-Ion Batteries Based on Time-Ratio Features. *Sustain. Energy Technol. Assess.* **2025**, *79*, 104364. [CrossRef]